AGU ADVANCING EARTH AND SPACE SCIENCES

Geophysical Research Letters

RESEARCH LETTER
10.1029/2024GL109246

Spatial and Seasonal Controls on Eddy Subduction in the Southern Ocean

Michael L. Chen[1] and **Oscar Schofield**[1]

[1]Department of Marine and Coastal Sciences, Rutgers University, New Brunswick, NJ, USA

Key Points:

- Eddy subduction in the Southern Ocean is observed as subsurface anomalies in spice and oxygen measured by autonomous profiling floats
- Spatial distribution is controlled by weak stratification and strong lateral buoyancy gradients, diagnosed using satellite altimetry
- Bio-optical proxies suggest that eddy subduction is most active in spring/early summer, driven by weak vertical stratification

Supporting Information:

Supporting Information may be found in the online version of this article.

Correspondence to:

O. Schofield,
oscar@marine.rutgers.edu

Citation:

Chen, M. L., & Schofield, O. (2024). Spatial and seasonal controls on eddy subduction in the Southern Ocean. *Geophysical Research Letters*, *51*, e2024GL109246. https://doi.org/10.1029/2024GL109246

Received 1 MAY 2024
Accepted 4 SEP 2024

Abstract Carbon export driven by submesoscale, eddy-associated vertical velocities ("eddy subduction"), and particularly its seasonality, remains understudied, leaving a gap in our understanding of ocean carbon sequestration. Here, we assess mechanisms controlling eddy subduction's spatial and seasonal patterns using 15 years of observations from BGC-Argo floats in the Southern Ocean. We identify signatures of eddy subduction as subsurface anomalies in temperature-salinity and oxygen. The anomalies are spatially concentrated near weakly stratified areas and regions with strong lateral buoyancy gradients diagnosed from satellite altimetry, particularly in the Antarctic Circumpolar Current's standing meanders. We use bio-optical ratios, specifically the chlorophyll *a* to particulate backscatter ratio (Chl/b_{bp}) to find that eddy subduction is most active in the spring and early summer, with freshly exported material associated with seasonally weak vertical stratification and increasing surface biomass. Climate change is increasing ocean stratification globally, which may weaken eddy subduction's carbon export potential.

Plain Language Summary Oceans play an important role in global climate by soaking up and sequestering atmospheric carbon dioxide. Photosynthetic activity at the surface turns carbon dioxide into organic carbon, and if this carbon leaves the surface to the deep ocean, it can be locked away from the atmosphere. One way this occurs is through the physical circulation associated with swirling eddies, which can rapidly transport organic carbon-rich surface waters and "inject" them into deep waters. However, we still don't fully understand the seasonal timing of this process, or what drives its spatial distribution. We investigated this in the Southern Ocean, which is very important to global climate, using data collected by drifting robots. We find that this process is the most active in regions where eddies drive strong surface stirring, and during the spring, when weak stratification allows injections to penetrate deep into the ocean. Because this process is poorly represented in climate models, these findings will improve our understanding of how the ocean absorbs carbon.

1. Introduction

Oceans play a critical role in regulating global climate by sequestering carbon from the atmosphere (Gruber et al., 2009). A key driver of this is the biological pump, a suite of processes that exports carbon from the ocean's surface to the interior, and is estimated to keep 1,300 Pg C sequestered from the atmosphere (Nowicki et al., 2022). The best understood mechanism is the biological gravitational pump, or the sinking of large particles out of the euphotic zone, which is estimated to comprise about 70% of global carbon export (Boyd et al., 2019; Nowicki et al., 2022). However, other mechanisms are increasingly being recognized (Boyd et al., 2019). These include transport by vertically migrating mesopelagic organisms (Bianchi et al., 2013), and physical processes such as carbon detrainment from shoaling mixed layers (the "mixed-layer pump"; Dall'Olmo et al., 2016; Lacour et al., 2019), large-scale water mass subduction (the "subduction pump"; Levy et al., 2013), and submesoscale vertical velocities associated with frontal boundaries and eddies (the "eddy subduction pump", or "ESP"; Omand et al., 2015; Resplandy et al., 2019). If these submesoscale vertical motions coincide with the presence of organic carbon in the surface ocean, carbon export can occur. During phytoplankton blooms, models and observations show that filaments of organic carbon-rich surface waters can be injected to depth along eddy peripheries (Davies et al., 2019; Omand et al., 2015).

Eddy subduction (henceforth, also "subduction") remains particularly understudied due to the challenges of observing submesoscale processes. In recent decades, submesoscale physics has emerged as a key driver of vertical exchange. Advances in numerical modeling have revealed a dynamic eddy field at horizontal scales of *O* (1–10) m, associated with ageostrophic vertical velocities reaching up to 100 m day^{-1}. These evolve on timescales

of O (1) days with a vertical extension of O (100) m, and strongly contribute to vertical tracer variability (Balwada et al., 2018; Capet et al., 2008; Klein & Lapeyre, 2009; Lapeyre & Klein, 2006; Lévy et al., 2012; Mahadevan & Tandon, 2006; Rosso et al., 2014). Mechanisms energizing these vertical submesoscale flows include surface frontogenesis (Held et al., 1995; Lapeyre & Klein, 2006; Rosso et al., 2015) and baroclinic instabilities within the mixed layer ("mixed layer instabilities"), which extract potential energy stored in lateral buoyancy gradients and deep mixed layers (Boccaletti et al., 2007; Callies et al., 2015, 2016; Erickson & Thompson, 2018).

Once subducted, parcels of water retain tracer signatures of their surface origins, including elevated oxygen and surface-like temperature-salinity (Davies et al., 2019; Omand et al., 2015). Recently, Llort et al. (2018) used these signatures to develop an algorithm that detects eddy subduction in BGC-Argo float profiles. This algorithm identified subsurface anomalies in two variables known to reflect recent subduction from the surface: apparent oxygen utilization (AOU) and spice, a temperature-salinity variable least-correlated with density, which helps identify water mass movement along isopycnals. These anomalies were often associated with elevated particulate organic carbon (POC), and were spatially located in energetic regions of the Southern Ocean (SO). Since then, this approach has enabled the identification of eddy subduction in regions such as the SO (Lacour et al., 2023), the North Atlantic (A. R. Johnson & Omand, 2021) and the Kuroshio Extension (Chen et al., 2021), and has generated estimates of eddy subduction's contribution to carbon export. However, these vary widely, ranging from up to 50% of exported POC during spring blooms, to as little as <5% (Davies et al., 2019; Llort et al., 2018; Omand et al., 2015; Resplandy et al., 2019; Stukel & Ducklow, 2017).

A critical knowledge gap is our poor understanding of eddy subduction's seasonality, which determines what kind of particles are exported and their sequestration potential, and is a major uncertainty in global carbon export calculations (Nowicki et al., 2022). Previous observational studies have mixed findings, detecting the most subduction events either during the summer (A. R. Johnson & Omand, 2021; Llort et al., 2018), spring (Chen et al., 2021), or throughout the year (Lacour et al., 2023). A challenge in assessing seasonality in float-based studies is determining the "age" of subduction events. A detected subsurface feature may have been subducted months ago, as AOU and spice anomalies may persist at depth for months (A. R. Johnson & Omand, 2021). To this end, ratios of bio-optical proxies are a promising tool to help "age" subducted material (Lacour et al., 2019), but have yet to be applied to basin-scale studies of eddy subduction.

Here, we use BGC-Argo floats in the SO to provide basin-scale analysis of eddy subduction's spatial distribution and seasonality, and tie them to physical mechanisms. For the first time, we integrate bio-optical ratios in a basin-scale eddy subduction study to more robustly address seasonality, and find a seasonal peak in the austral spring, associated with weak vertical stratification and increasing surface biomass. Integrating satellite altimetry, we find that strong lateral buoyancy gradients and weak stratification shape eddy subduction's spatial distribution. This work demonstrates the utility of bio-optical ratios in observational carbon export studies. Our mechanistic findings are also an important step toward resolving when and where submesoscale carbon export occurs, an urgent need in understanding the ocean's role in carbon cycling and climate change.

2. Data and Methods

2.1. Float Data

BGC-Argo float data are from the Southern Ocean Carbon and Climate Observations and Modeling (SOCCOM) program. Floats conduct 2,000 m vertical profiles every 10 days, and drift at a parking depth of 1,000 m. Vertical sampling frequency varies between two float types: Navis floats sample every 2 m in the upper 1,000 m. APEX floats sample less frequently, with resolution decreasing with depth. Sampling schemes are described in Johnson et al. (2017), as well as processing of bio-optical parameters, including particulate backscatter at 700 nm (b_{bp}), which is used to derive POC, and chlorophyll a fluorescence, which is used to derive chlorophyll a concentrations (Chl). Quality control procedures for all other variables are described in Maurer et al. (2021). Only data flagged as "good" were used.

Variables such as conservative temperature (CT) and absolute salinity (S_A) were derived using the Thermodynamic Equation of Seawater 2010 (TEOS-10; McDougall & Barker, 2011). Spice was calculated as a function of CT and S_A, following McDougall & Krzysik, 2015. AOU was calculated as ($AOU = O_2^{sat} - O_2^{obs}$), where O_2^{sat} is the oxygen saturation concentration calculated using the coefficients of Garcia and Gordon (1992, 1993), and

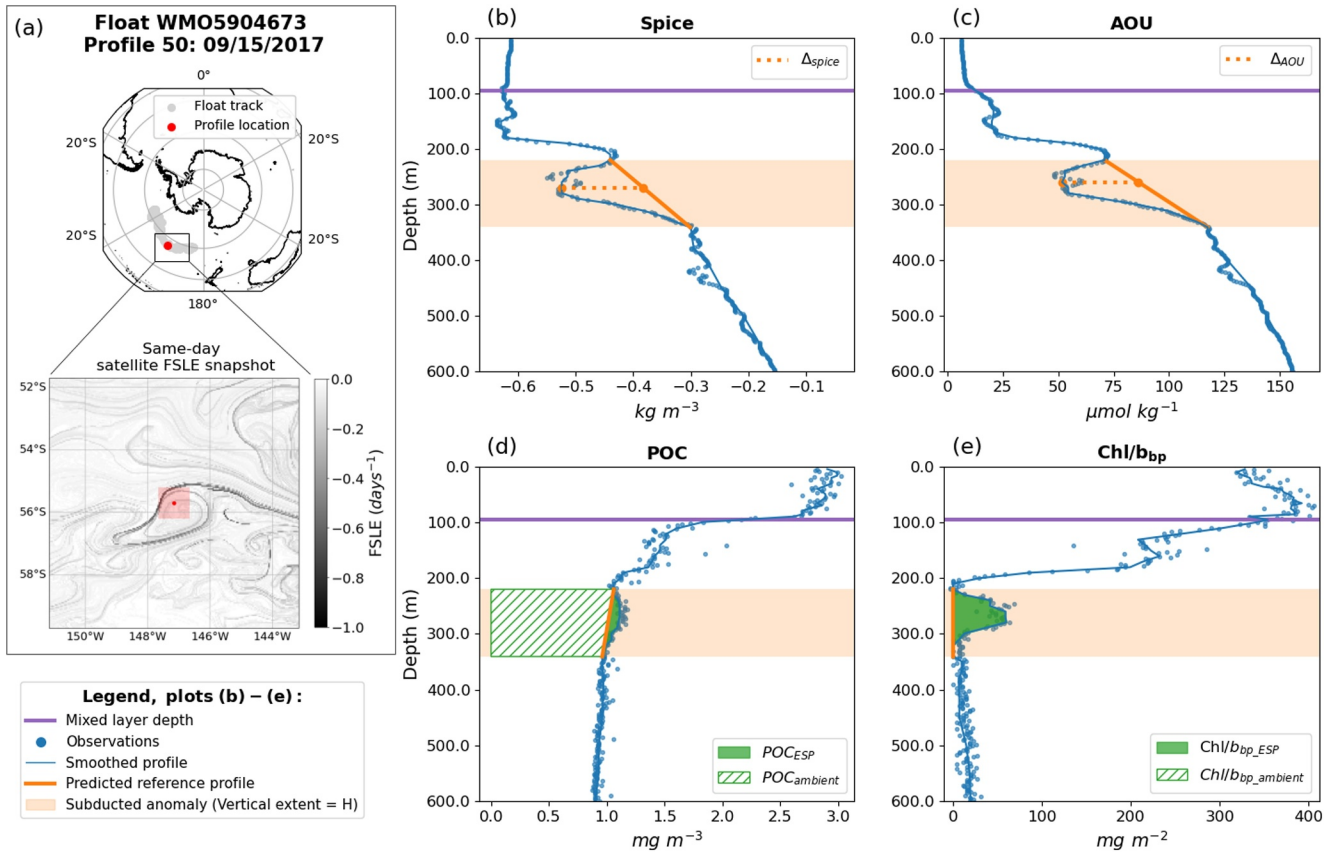

Figure 1. Example of an eddy subduction anomaly detected in a float profile. (a) Map depicting float track and profile location (red circle). Inset shows the same-day surface FSLE field. Red circle = profile location. Shaded red box = the 1° × 1° area used to retrieve the strongest FSLE in the profile's vicinity. The float's vertical profiles are shown in (b)-(d), with the MLD indicated by a purple line. Blue lines depict smoothed profiles. The shaded orange band indicates H, the vertical extent of the subduction anomaly. (b) Spice profile. Dotted orange line shows Δ_{spice} at depth h_{spice}, or the difference between the observed value and the calculated reference value (orange circles). The reference profile is shown by the orange line. (c) AOU profile, with reference profile and Δ_{AOU}, similar to the spice profile. (d) POC profile. Shaded green region: POC_{ESP}, the integrated quantity of subduction-driven POC. Hatched region: $POC_{ambient}$, the subtracted, integrated quantity of ambient POC. (e) Chl/b_{bp} ratio profile. Shaded green area: Chl/b_{bp_ESP}, similar to POC. Hatched region: Chl/$b_{bp\_ambient}$, not visible because values are roughly 0.

O_2^{obs} is the observed dissolved oxygen concentration. Mixed layer depth was defined using a density difference threshold of 0.03 kg m^{-3} from the surface, and buoyancy frequency squared (N^2) was calculated using TEOS-10.

2.2. Eddy Subduction Anomaly Detection

We identified eddy subduction anomalies in float profiles using an algorithm adapted from Chen et al. (2021) and Llort et al. (2018). An example is shown in Figure 1, detected on the periphery of a mesoscale eddy (Figure 1a). We considered profiles between 30°S and 65°S, and discarded profiles with surface salinity >35 psu, following Llort et al. (2018). We also only considered profiles where the median spice value in the mixed layer was lower than that at 600 m, as increasing spice with depth in the upper 1,000 m is characteristic of SO waters (Tailleux, 2021). Navis floats were down-sampled by selecting data at APEX sampling depths, allowing for comparable vertical resolution. Profiles were vertically smoothed with a 3-bin rolling median. The total dataset contained 9,354 profiles with temperature, salinity, and oxygen collected from February 2008 through August 2023, with 8,545 measuring Chl and b_{bp}.

For each smoothed profile, we identified co-occurring peaks in spice and AOU between the MLD and 600 m depth (relative minima found within 30 m of each other, at depths h_{spice} and h_{AOU}; Figures 1b and 1c). We then defined reference profiles to simulate "background", ambient values in the absence of subduction (orange lines, Figures 1b and 1c). An initial guess for the reference profile is defined as the straight line between the maximum values above and below each peak (within 100 m in either direction), following Chen et al., 2021. The top and

bottom boundaries of this initial guess are then iteratively adjusted to ensure the boundaries are coherent (see Figure S1 in Supporting Information S1). We then calculated the difference between the observed value and the calculated reference value at h_{spice} and h_{AOU}, yielding Δ_{spice} and Δ_{AOU}, respectively (Figures 1b and 1c). Peaks were classified as eddy subduction pump anomalies ("ESP anomalies") if $\Delta_{spice} < -0.05$ kg/m^3 and $\Delta_{AOU} < -8$ μmol/kg, following Llort et al. (2018). The anomaly depth was defined at h_{AOU}, and the vertical extent of the anomaly (H) was defined as the extent of the reference profile for AOU. We discarded anomalies found within 100 m of the MLD in order to avoid misidentifying detrainment from shoaling mixed layers (Lacour et al., 2019).

We then sought to quantify biogeochemical values (e.g., POC, Chl/b_{bp}, AOU) associated with anomalies, and isolate the portion driven by subduction, versus by ambient processes such as gravitational sinking. Taking POC as an example, we first calculated the total value by integrating the observed profiles over the vertical span of the anomaly (H):

$$POC_{ESP_{total}} = \int_{H_{bottom}}^{H_{top}} POC_{observed} \quad (1)$$

We estimated the ambient value by integrating through the reference profile (hatched regions in Figures 1d and 1e):

$$POC_{ESP_{ambient}} = \int_{H_{bottom}}^{H_{top}} POC_{reference} \quad (2)$$

From the ambient and total values, we calculated the subduction-driven value (green shaded regions in Figures 1d and 1e):

$$POC_{ESP} = POC_{ESP_{total}} - POC_{ESP_{ambient}} \quad (3)$$

Finally, we normalized these by H to yield the depth-averaged, subduction-driven value in the original units:

$$POC_{ESP_{avg}} = \frac{POC_{ESP}}{H} \quad (4)$$

2.3. Satellite Data

Finite-size Lyapunov Exponents (FSLEs) were downloaded from AVISO+. FSLEs describe stretching and compression by quantifying the exponential rate of separation (λ) of neighboring particles advected in a flow field: $\lambda(d_0,d_f) = \frac{1}{t}log\left(\frac{d_f}{d_0}\right)$, where d_0 and d_f are the initial and final distances between the particles, respectively, and t is the time it takes for the particles to reach d_f (d'Ovidio et al., 2004). The AVISO + product uses daily, altimetry-derived geostrophic velocity fields to advect particles backward-in-time, so FSLEs are negative, with stronger negative values indicating stronger stretching; these FSLE ridges indicate transport barriers and are preferentially located between eddy cores (Siegelman, Klein, Thompson, et al., 2020).

3. Results and Discussion

3.1. Spatial Distribution of Eddy Subduction

The BGC-Argo dataset provides basin-wide spatial coverage of the SO over 15 years. We find eddy subduction anomalies in 4.4% of profiles, defined as coherent, negative mesopelagic anomalies in spice and AOU (Figures 1b and 1c), frequently associated with positive anomalies in bio-optical parameters (67% with positive b_{bp}, 56% with positive Chl a) (Figures 1d and 1e). These anomalies are spatially concentrated around the Polar Front and Antarctic Circumpolar Current (ACC), consistent with Llort et al. (2018) (Figure 2a). Also consistent with Llort et al. (2018) and Dove et al. (2022), their circumpolar distribution is uneven, with most detected in the ACC's standing meander regions: the Eastern Pacific Rise, the Kerguelen, Crozet, and Campbell Plateaus, and the Drake Passage. These regions are known for enhanced eddy kinetic energy (EKE) and vertical exchange (Dove

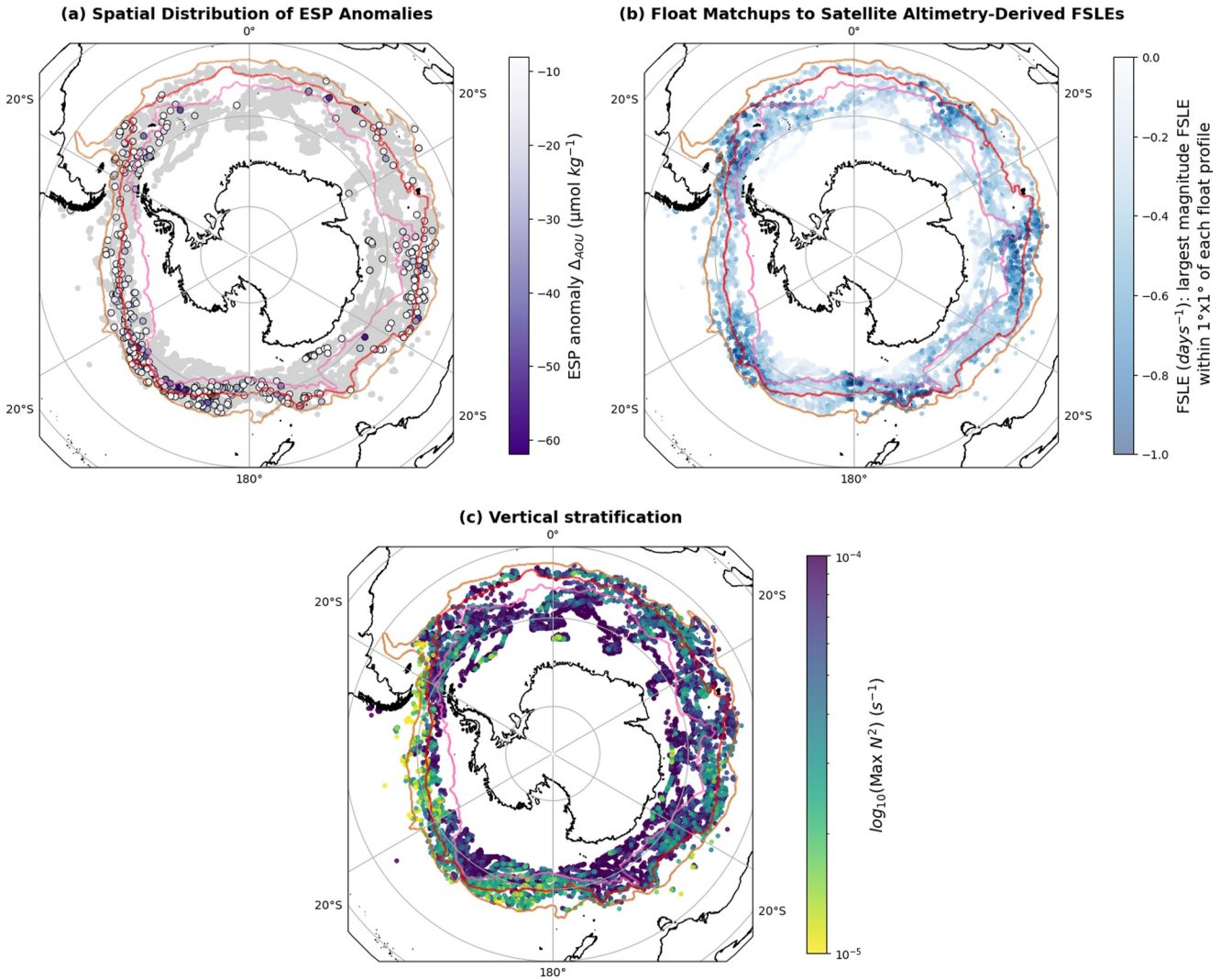

Figure 2. Maps of the float dataset. Colored lines indicate front locations as defined by mean dynamic topography from satellite altimetry (Park & Durand, 2019): orange = Subantarctic Front (SAF); red = Polar Front (PF); pink = Southern ACC Front (SACCF). (a) Locations of eddy subduction anomalies across the SO. Gray circles indicate all profiles considered in the analysis. Purple-scale colored circles indicate detected ESP anomalies, colored by the magnitude of Δ_{AOU}. (b) Spatial distribution of FSLEs. Each point is a satellite matchup to a float profile, showing the strongest FSLE within 1° × 1° of each profile. (c) Spatial distribution of vertical stratification (maximum N^2) in each float profile, and displayed on a log-scale. The colorscale maximum is limited to 10^{-4} (roughly the median of the maximum N^2 distribution; see Figure 4d) to emphasize variation in the lower half of the distribution.

et al., 2022), as the ACC interacts with underwater topography and generates mesoscale eddies that strain surface density fields and energize submesoscale motions (Rosso et al., 2015).

To better assess spatial distribution, we use altimetry-derived FSLEs. FSLEs are elevated within the ACC's standing meanders (Dove et al., 2022), and strong FSLEs are co-located with strong, deep-reaching submesoscale lateral buoyancy gradients and intense vertical velocities (Siegelman, et al., 2020a, 2020b). To assess whether a given float profile was in the vicinity of submesoscale fronts, we matched each profile with its same-day satellite FSLE field and identified the strongest FSLE within the surrounding 1° × 1° area (e.g., within the red square in Figure 1a). These matchups are displayed in Figure 2b and show the ACC's standing meanders as submesoscale hotspots, largely congruent with the distribution of eddy subduction anomalies.

However, groups of anomalies are detected in comparatively quiescent regions in between the standing meanders, such as 60°W–120°W and 150°W–180°W (Figures 2a and 2b). Although stratification shows a less dramatic spatial pattern, many profiles in these regions have comparatively weak stratification (yellow colors in Figure 2c), which may influence eddy subduction's spatial distribution by allowing deeper vertical penetration of

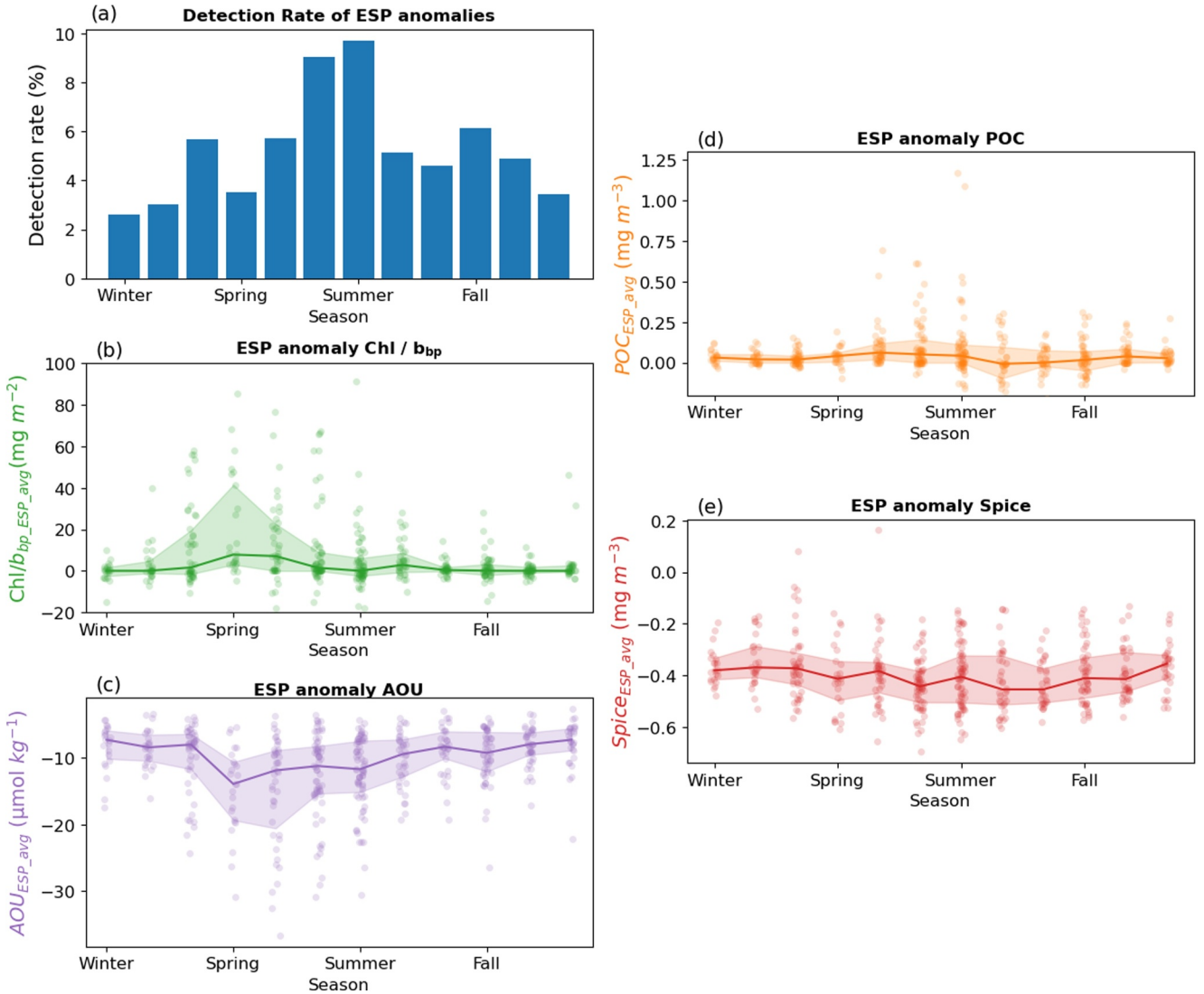

Figure 3. Seasonal patterns across observed ESP anomalies. *X*-axis ticks correspond to [June, Sept, Dec, Mar]. (a) Detection rate of ESP anomalies per month, normalized by the total number of profiles per month. Plots (b)-(e) show seasonality of depth-averaged, subduction-driven properties within ESP anomalies. Line plots depict medians, with shaded regions indicating interquartile ranges. Overlain strip plots show individual data points. (b) $POC_{\_ESP\_avg}$, (c) $Chl/b_{bp\_ESP\_avg}$, (d) $AOU_{\_ESP\_avg}$, (e) $spice_{\_ESP\_avg}$. Axis limits in (b) and (d) display 98% of data points.

submesoscale flows (Callies et al., 2016; Erickson & Thompson, 2018). These mechanistic relationships will be further explored in Section 3.3.

3.2. Seasonality of Eddy Subduction

We detect subduction anomalies more frequently during summer months (Figure 3a). However, our method only identifies subsurface anomalies after subduction occurs, and these anomalies may persist for months at depth afterward (A. R. Johnson & Omand, 2021).

To better assess the timing and "age" of subduction, we integrate bio-optical ratios, particularly Chl/b_{bp} — the ratio of chlorophyll *a* to particulate backscatter. At the surface, this ratio reflects phytoplankton photophysiology, community composition, and particle assemblage (Barbieux et al., 2018; Cetinić et al., 2015; Rembauville et al., 2017). However, beneath the mixed layer, it can be a proxy for the freshness of exported material; after particulate material leaves the mixed layer, Chl/b_{bp} decays by a power law as phytoplankton pigments degrade (Lacour et al., 2019). Calculating a precise age for a given Chl/b_{bp} observation at depth is difficult; however, we

argue it is a rough but robust proxy for particle age in the mesopelagic SO. First, values in the surface mixed layer and in the mesopelagic are distinct: over an order of magnitude lower in the mesopelagic (Figure S2 in Supporting Information S1); thus, high mesopelagic values likely indicate recent surface origins. Second, ambient Chl/b_{bp} at depth shows strong seasonality, with a summertime peak that is tightly coupled to seasonal POC maxima at the surface and at depth (Figure S3 in Supporting Information S1), reflecting a pulse of fresh sinking organic matter after surface phytoplankton blooms. By contrast, Chl/b_{bp} at the surface shows weak seasonality (Figure S3 in Supporting Information S1), controlled to first-order in the SO by community composition (Barbieux et al., 2018); thus, seasonality in surface Chl/b_{bp} is unlikely to strongly influence values at depth. Together, these suggest that high Chl/b_{bp} values at depth are largely controlled by how recently material left the surface.

Within subduction anomalies, Chl/$b_{bp\_ESP\_avg}$ is frequently elevated relative to ambient mesopelagic waters, indicating freshly subducted phytoplankton biomass (Figure 1e). It has a distinct seasonal cycle, with the highest values (the most freshly subducted material), occurring during the spring and early summer (Figure 3b). AOU (as $AOU_{\_ESP\_avg}$) shows a similar seasonality, with the most negative values occurring during the spring (Figure 3c), indicating less respiration, or "aging", has occurred. Springtime events are also slightly closer to the mixed layer, consistent with more recent isolation (Figure S4 in Supporting Information S1). By comparison, the seasonal cycle of eddy-subducted POC ($POC_{\_ESP\_avg}$) is weak, although the highest $POC_{\_ESP\_avg}$ event outliers are detected in the summer (Figure 3d). This suggests that although eddy subduction may be most active in the spring, these events may not necessarily export large amounts of POC. Interestingly, $spice_{\_ESP\_avg}$, a purely physical variable, does not show a seasonal cycle (Figure 3e), suggesting that the relative roles of physics versus respiration in dissipating features after subduction need to be untangled through high-resolution sampling.

Most importantly, the seasonal cycles we show are distinct from those of other processes in the mesopelagic and from surface Chl/b_{bp}, lending confidence that they reveal patterns unique to eddy subduction. For example, ambient mesopelagic POC and Chl/b_{bp} are tightly coupled to the summertime peak in surface POC (Figure S3 in Supporting Information S1), and is likely mediated by the gravitational sinking of large particles from surface blooms (Figure S5 in Supporting Information S1). Eddy subduction's springtime peak thus represents a distinct seasonality, and could facilitate export of different pools of carbon present in the spring (i.e., dissolved or inorganic carbon, which we do not discuss here). Future work should investigate this seasonality's implications for carbon sequestration.

3.3. Physical and Biological Mechanisms Controlling Spatial and Seasonal Patterns

Next, we link the previously discussed spatial and seasonal patterns to biological and physical processes required for eddy subduction of POC: POC availability at the ocean's surface, strong lateral buoyancy gradients, deep mixed layers, and weak vertical stratification (Callies et al., 2016; Erickson & Thompson, 2018; Fox-Kemper et al., 2008). We define vertical stratification as the maximum N^2 over the entire profile, as well-defined mixed layers often do not exist in energetic regions (Erickson & Thompson, 2018). However, our results are unaffected if we instead use N^2 at the base of the mixed layer (Figure S6 in Supporting Information S1).

Examining seasonal cycles in these variables, spring/early summer emerges as a period conducive to eddy subduction, with an overlap of deep mixed layers, weak vertical stratification, and increasing surface POC (Figure 4a). This aligns with the seasonality discussed in Section 3.2. Interestingly, altimetry-derived FSLEs do not show a seasonal cycle here (Figure 4b), suggesting that lateral buoyancy gradients in this region may not drive eddy subduction's seasonality.

Statistical distributions of float profiles provide further insights. Profiles with subduction anomalies are shifted towards higher surface POC (Figure 4c), demonstrating that carbon must be available to be exported. Similarly, profiles with subduction anomalies are shifted towards weakly stratified water columns (Figure 4d). Profiles with anomalies in the top quartile of Chl/$b_{bp\_ESP\_avg}$ values, likely most recently subducted, are even more weakly stratified. Direct comparison of maximum N^2 to Chl/$b_{bp\_ESP\_avg}$ suggests that weak stratification is a prerequisite for detecting recent eddy subduction (Figure S7 in Supporting Information S1). Interestingly, despite its strong seasonality, mixed layer depth shows little effect–distributions are similar between profiles with and without subduction anomalies (Figure 4e). Conversely, although FSLEs do not show seasonality, profiles with subduction anomalies are strongly shifted towards stronger nearby FSLEs (Figure 4f).

10.1029/2024GL109246

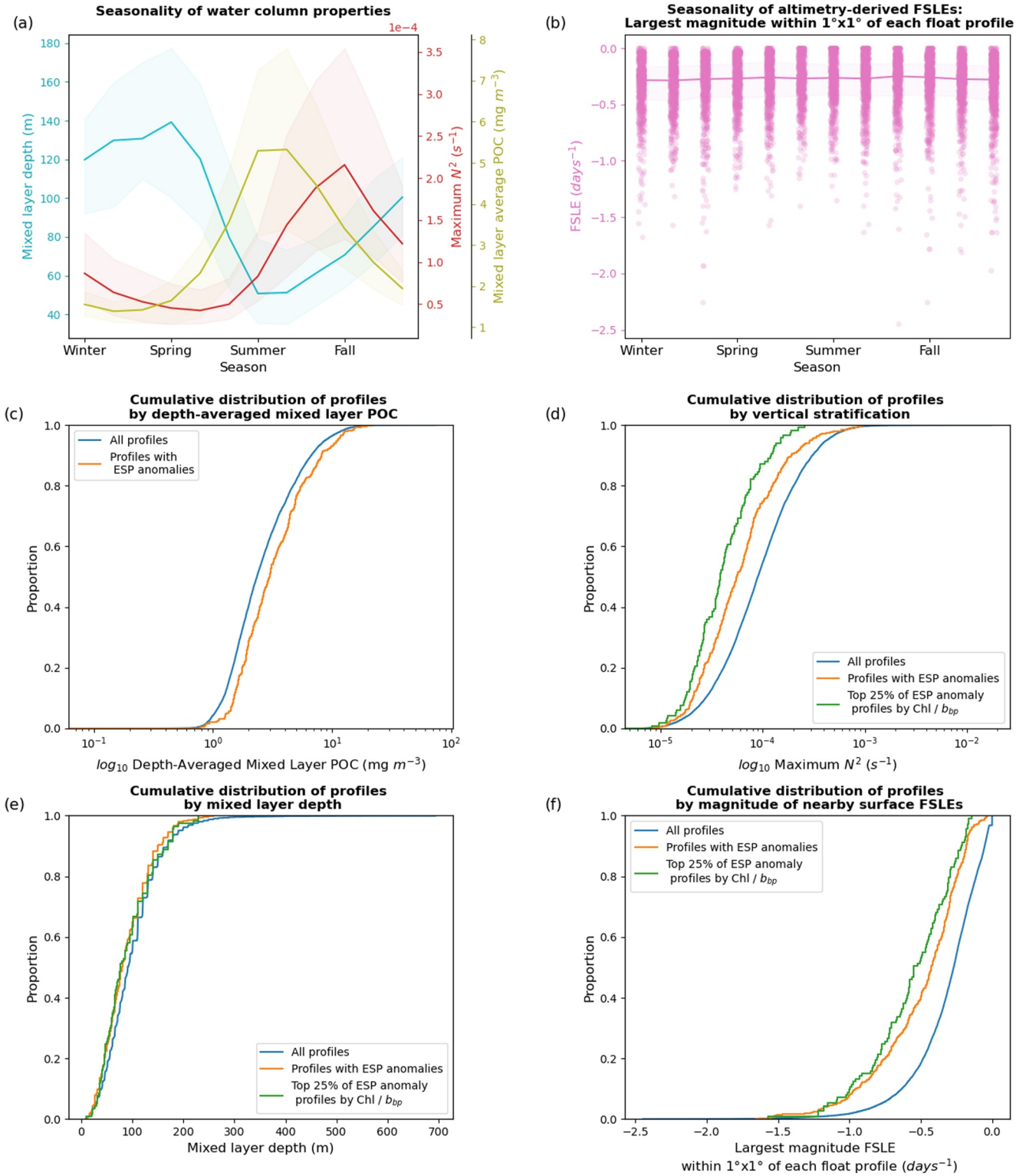

Figure 4. Mechanisms driving eddy subduction. (a) Seasonality of water column properties for all float profiles, showing MLD (blue), maximum N^2 (red), and depth-averaged POC within the surface mixed layer (olive). The line plot depicts medians, with shaded regions indicating interquartile ranges. (b) Seasonality of altimetry-derived FSLE magnitudes. The strip plot shows satellite matchups to each float profile, showing the strongest FSLE within 1° × 1°. Line plot as in (a). (c)-(f) Cumulative distribution plots of profiles by various mechanistic variables. Each curve represents the cumulative proportion of observations falling below the corresponding *x*-axis value. Colors indicate all profiles (blue), only profiles with ESP anomalies (orange), and only profiles with ESP anomalies with the highest 25% Chl/$b_{bp\_ESP\_avg}$ values (green) (c) Depth-averaged mixed layer POC (log_{10}) (d) Maximum N^2 (log_{10}). (e) Mixed layer depth. (f) Magnitude of the strongest altimetry-derived FSLE within a 1° × 1° area.

These analyses indicate that in the SO, strong lateral buoyancy gradients and weak vertical stratification exert significant physical controls on eddy subduction. The spatial analyses in Section 3.1 suggest that these drive eddy subduction's concentration in standing meanders and weakly stratified areas. Meanwhile, the seasonal analyses in Sections 3.2 and 3.3 suggest that vertical stratification and seasonal availability of surface POC are dominant drivers of seasonality. Mixed layer depth appears to exert little influence. Consistent with Stommel's Demon theory, weak springtime stratification may act as a seasonal trapdoor in areas prone to submesoscale motions, determining whether they can export material beneath the mixed layer (Stommel, 1979).

4. Conclusions

Our work has broad implications for our understanding of carbon export and submesoscale dynamics, and emphasizes open questions for the community. First, we identify a seasonal cycle in eddy subduction, which has remained unresolved in global carbon export calculations (Nowicki et al., 2022). Future work should assess global variability beyond the SO, and assess the implications of seasonality on what pools of carbon are exported and their sequestration potential. Second, we highlight the utility of bio-optical ratios in studies of carbon export. However, high-resolution sampling is necessary to quantify the evolution and aging of tracers after subduction. Third, we emphasize the power of contextualizing subsurface float observations with Lagrangian surface diagnostics, such as satellite FSLEs. Finally, we identify strong lateral buoyancy gradients, weak vertical stratification, and POC availability as spatiotemporal controls on vertical exchange in the SO. Future investigation should untangle specific physical mechanisms (i.e., frontogenesis vs. instabilities; Archer et al., 2020; Callies et al., 2015; Erickson & Thompson, 2018; Klein & Lapeyre, 2009; Rosso et al., 2015) and use these parameters to model when and where submesoscale carbon export occurs. Finally, climate change is increasing stratification strength across global oceans (Sallée et al., 2021), potentially decreasing eddy subduction's export potential, and underscoring the importance of understanding this process's role in ocean carbon sequestration.

Data Availability Statement

Float data were downloaded from the UCSD SOCCOM and GO-BGC data archive. Our analyses use the delayed-mode, quality controlled, low-resolution snapshot from 2023 to 08-28 (Riser et al., 2023). Altimetry-derived FSLEs were produced by Ssalto/Duacs in collaboration with LOcean and CTOH and distributed by AVISO+, with support from CNES (https://www.aviso.altimetry.fr/en/data/products/value-added-products/fsle-finite-size-lyapunov-exponents.html). Analyses were conducted in Python 3.8.17 using Xarray version 2022.11.0, available under the Apache license at https://docs.xarray.dev/ (The Xarray Development Team, 2022); GSW version 3.6.17, available under the GSW License at https://www.TEOS-10.org (McDougall & Barker, 2011); and Pandas version 1.5.3, available under the BSD 3-Clause "New" or "Revised" License at https://pandas.pydata.org (The Pandas Development, 2023). Figures were plotted using Matplotlib version 3.7.1, available under the Matplotlib license at https://matplotlib.org (The Matplotlib Development Team, 2023); Seaborn version 0.12, available under the BSD 3-Clause "New" or "Revised" License at https://seaborn.pydata.org (The Seaborn Development Team, 2022); and Cartopy version 0.21.1, available under the BSD-3 Clause License at https://scitools.org.uk/cartopy/ (The Cartopy Development Team, 2022). The software associated with this manuscript for data processing and analysis is licensed under MIT and published on GitHub https://github.com/mchen96/southern_ocean_eddy_subduction/, and can be run in a zero-install environment on the cloud at https://mybinder.org/v2/gh/mchen96/southern_ocean_eddy_subduction/main (M. Chen, 2024).

Acknowledgments
The authors are grateful for the comments of anonymous reviewers who greatly improved the manuscript, and for conversations with Joan Llort, Shuangling Chen, Léo Lacour, Laure Resplandy, Kathleen Abbott, Lily Dove, Mara Freilich, and Jackie Veatch. Float data were collected and made freely available by the SOCCOM Project funded by the National Science Foundation, Division of Polar Programs (NSF PLR-1425989 and OPP-1936222), supplemented by NASA, and by the International Argo Program and the NOAA programs that contribute to it. The Argo Program is part of the Global Ocean Observing System. M.L. Chen acknowledges NASA Grant 80NSSC22K1451. O. Schofield acknowledges NASA Grant 80NSSC21K0969.

References

Archer, M., Schaeffer, A., Keating, S., Roughan, M., Holmes, R., & Siegelman, L. (2020). Observations of submesoscale variability and frontal subduction within the mesoscale eddy field of the tasman sea. *Journal of Physical Oceanography*, *50*(5), 1509–1529. https://doi.org/10.1175/JPO-D-19-0131.1

Balwada, D., Smith, K. S., & Abernathey, R. (2018). Submesoscale vertical velocities enhance tracer subduction in an idealized antarctic circumpolar current. *Geophysical Research Letters*, *45*(18), 9790–9802. https://doi.org/10.1029/2018GL079244

Barbieux, M., Uitz, J., Bricaud, A., Organelli, E., Poteau, A., Schmechtig, C., et al. (2018). Assessing the variability in the relationship between the particulate backscattering coefficient and the chlorophyll *a* concentration from a global biogeochemical-argo database. *Journal of Geophysical Research: Oceans*, *123*(2), 1229–1250. https://doi.org/10.1002/2017JC013030

Bianchi, D., Stock, C., Galbraith, E. D., & Sarmiento, J. L. (2013). Diel vertical migration: Ecological controls and impacts on the biological pump in a one-dimensional ocean model. *Global Biogeochemical Cycles*, *27*(2), 478–491. https://doi.org/10.1002/gbc.20031

Boccaletti, G., Ferrari, R., & Fox-Kemper, B. (2007). Mixed layer instabilities and restratification. *Journal of Physical Oceanography*, *37*(9), 2228–2250. https://doi.org/10.1175/JPO3101.1

Boyd, P. W., Claustre, H., Levy, M., Siegel, D. A., & Weber, T. (2019). Multi-faceted particle pumps drive carbon sequestration in the ocean. *Nature*, *568*(7752), 327–335. https://doi.org/10.1038/s41586-019-1098-2

Callies, J., Ferrari, R., Klymak, J. M., & Gula, J. (2015). Seasonality in submesoscale turbulence. *Nature Communications*, *6*(1), 6862. https://doi.org/10.1038/ncomms7862

Callies, J., Flierl, G., Ferrari, R., & Fox-Kemper, B. (2016). The role of mixed-layer instabilities in submesoscale turbulence. *Journal of Fluid Mechanics*, *788*, 5–41. https://doi.org/10.1017/jfm.2015.700

Capet, X., McWilliams, J. C., Molemaker, M. J., & Shchepetkin, A. F. (2008). Mesoscale to submesoscale transition in the California current System. Part I: Flow structure, eddy flux, and observational tests. *Journal of Physical Oceanography*, *38*(1), 29–43. https://doi.org/10.1175/2007JPO3671.1

Cetinić, I., Perry, M. J., D'Asaro, E., Briggs, N., Poulton, N., Sieracki, M. E., & Lee, C. M. (2015). A simple optical index shows spatial and temporal heterogeneity in phytoplankton community composition during the 2008 North Atlantic Bloom Experiment. *Biogeosciences*, *12*(7), 2179–2194. https://doi.org/10.5194/bg-12-2179-2015

Chen, M. (2024). Southern Ocean eddy subduction (version v1.0.3). [software]. https://doi.org/10.5281/zenodo.10999661. *Zenodo*.

Chen, S., Wells, M. L., Huang, R. X., Xue, H., Xi, J., & Chai, F. (2021). Episodic subduction patches in the western North Pacific identified from BGC-Argo float data. *Biogeosciences*, *18*(19), 5539–5554. https://doi.org/10.5194/bg-18-5539-2021

Dall'Olmo, G., Dingle, J., Polimene, L., Brewin, R. J. W., & Claustre, H. (2016). Substantial energy input to the mesopelagic ecosystem from the seasonal mixed-layer pump. *Nature Geoscience*, *9*(11), 820–823. https://doi.org/10.1038/ngeo2818

Davies, A. R., Veron, F., & Oliver, M. J. (2019). Biofloat observations of a phytoplankton bloom and carbon export in the Drake Passage. *Deep Sea Research Part I: Oceanographic Research Papers*, *146*, 91–102. https://doi.org/10.1016/j.dsr.2019.02.004

Dove, L. A., Balwada, D., Thompson, A. F., & Gray, A. R. (2022). Enhanced ventilation in energetic regions of the antarctic circumpolar current. *Geophysical Research Letters*, *49*(13), e2021GL097574. https://doi.org/10.1029/2021GL097574

d'Ovidio, F., Fernández, V., Hernández-García, E., & López, C. (2004). Mixing structures in the Mediterranean Sea from finite-size Lyapunov exponents. *Geophysical Research Letters*, *31*(17), 2004GL020328. https://doi.org/10.1029/2004GL020328

Erickson, Z. K., & Thompson, A. F. (2018). The seasonality of physically driven export at submesoscales in the northeast atlantic ocean. *Global Biogeochemical Cycles*, *32*(8), 1144–1162. https://doi.org/10.1029/2018GB005927

Fox-Kemper, B., Ferrari, R., & Hallberg, R. (2008). Parameterization of mixed layer eddies. Part I: Theory and diagnosis. *Journal of Physical Oceanography*, *38*(6), 1145–1165. https://doi.org/10.1175/2007JPO3792.1

Garcia, H. E., & Gordon, L. I. (1992). Oxygen solubility in seawater: Better fitting equations. *Limnology & Oceanography*, *37*(6), 1307–1312. https://doi.org/10.4319/lo.1992.37.6.1307

Garcia, H. E., & Gordon, L. I. (1993). Erratum: Oxygen solubility in seawater: Better fitting equations. *Limnology & Oceanography*, *38*, 656.

Gruber, N., Gloor, M., Mikaloff Fletcher, S. E., Doney, S. C., Dutkiewicz, S., Follows, M. J., et al. (2009). Oceanic sources, sinks, and transport of atmospheric CO2. *Global Biogeochemical Cycles*, *23*(1). n/a-n/a. https://doi.org/10.1029/2008GB003349

Held, I. M., Pierrehumbert, R. T., Garner, S. T., & Swanson, K. L. (1995). Surface quasi-geostrophic dynamics. *Journal of Fluid Mechanics*, *282*, 1–20. https://doi.org/10.1017/S0022112095000012

Johnson, A. R., & Omand, M. M. (2021). Evolution of a subducted carbon-rich filament on the edge of the North Atlantic gyre. *Journal of Geophysical Research: Oceans*, *126*(2). https://doi.org/10.1029/2020JC016685

Johnson, K. S., Plant, J. N., Coletti, L. J., Jannasch, H. W., Sakamoto, C. M., Riser, S. C., et al. (2017). Biogeochemical sensor performance in the SOCCOM profiling float array. *Journal of Geophysical Research: Oceans*, *122*(8), 6416–6436. https://doi.org/10.1002/2017JC012838

Klein, P., & Lapeyre, G. (2009). The oceanic vertical pump induced by mesoscale and submesoscale turbulence. *Annual Review of Marine Science*, *1*(1), 351–375. https://doi.org/10.1146/annurev.marine.010908.163704

Lacour, L., Briggs, N., Claustre, H., Ardyna, M., & Dall'Olmo, G. (2019). The intraseasonal dynamics of the mixed layer pump in the subpolar North Atlantic ocean: A biogeochemical-argo float approach. *Global Biogeochemical Cycles*, *33*(3), 266–281. https://doi.org/10.1029/2018GB005997

Lacour, L., Llort, J., Briggs, N., Strutton, P. G., & Boyd, P. W. (2023). Seasonality of downward carbon export in the Pacific Southern Ocean revealed by multi-year robotic observations. *Nature Communications*, *14*(1), 1278. https://doi.org/10.1038/s41467-023-36954-7

Lapeyre, G., & Klein, P. (2006). Dynamics of the upper oceanic layers in terms of surface quasigeostrophy theory. *Journal of Physical Oceanography*, *36*(2), 165–176. https://doi.org/10.1175/JPO2840.1

Levy, M., Bopp, L., Karleskind, P., Resplandy, L., Ethe, C., & Pinsard, F. (2013). Physical pathways for carbon transfers between the surface mixed layer and the ocean interior. *Global Biogeochemical Cycles*, *27*(4), 1001–1012. https://doi.org/10.1002/gbc.20092

Lévy, M., Ferrari, R., Franks, P. J. S., Martin, A. P., & Rivière, P. (2012). Bringing physics to life at the submesoscale. *Geophysical Research Letters*, *39*(14), 2012GL052756. https://doi.org/10.1029/2012GL052756

Llort, J., Langlais, C., Matear, R., Moreau, S., Lenton, A., & Strutton, P. G. (2018). Evaluating southern Ocean Carbon eddy-pump from biogeochemical-argo floats. *Journal of Geophysical Research: Oceans*, *123*(2), 971–984. https://doi.org/10.1002/2017JC012861

Mahadevan, A., & Tandon, A. (2006). An analysis of mechanisms for submesoscale vertical motion at ocean fronts. *Ocean Modelling*, *14*(3–4), 241–256. https://doi.org/10.1016/j.ocemod.2006.05.006

Maurer, T. L., Plant, J. N., & Johnson, K. S. (2021). Delayed-mode quality control of oxygen, nitrate, and pH data on SOCCOM biogeochemical profiling floats. *Frontiers in Marine Science*, *8*, 683207. https://doi.org/10.3389/fmars.2021.683207

McDougall, T. J., & Barker, P. M. (2011). Getting started with TEOS-10 and the Gibbs seawater (GSW) oceanographic toolbox. *SCOR/IAPSO WG*, *127*, 1–28.

McDougall, T. J., & Krzysik, O. A. (2015). Spiciness. *Journal of Marine Research*, *73*(5), 141–152. https://doi.org/10.1357/002224015816665589

Nowicki, M., DeVries, T., & Siegel, D. A. (2022). Quantifying the carbon export and sequestration pathways of the oceanocean's biological carbon pump. *Global Biogeochemical Cycles*, *36*(3), e2021GB007083. https://doi.org/10.1029/2021GB007083

Omand, M. M., D'Asaro, E. A., Lee, C. M., Perry, M. J., Briggs, N., Cetinić, I., & Mahadevan, A. (2015). Eddy-driven subduction exports particulate organic carbon from the spring bloom. *Science*, *348*(6231), 222–225. https://doi.org/10.1126/science.1260062

Park, Y.-H., & Durand, I. (2019). Altimetry-drived antarctic circumpolar current fronts. [Dataset]. https://doi.org/10.17882/59800. *SEANOE*.

Rembauville, M., Briggs, N., Ardyna, M., Uitz, J., Catala, P., Penkerc'h, C., et al. (2017). Plankton assemblage estimated with BGC-argo floats in the Southern Ocean: Implications for seasonal Successions and particle export: Plankton assemblage bgc-argo. *Journal of Geophysical Research: Oceans*, *122*(10), 8278–8292. https://doi.org/10.1002/2017JC013067

Resplandy, L., Lévy, M., & McGillicuddy, D. J. (2019). Effects of eddy-driven subduction on ocean biological carbon pump. *Global Biogeochemical Cycles*, *33*(8), 1071–1084. https://doi.org/10.1029/2018GB006125

Riser, S. C., Talley, L. D., Wijffels, S. E., Nicholson, D., Purkey, S., Takeshita, Y., et al. (2023). Southern Ocean carbon and climate observations and modeling (SOCCOM) and Global Ocean biogeochemistry (GO-BGC) biogeochemical-argo float data archive. *UC San Diego Library Digital Collections*. [Dataset]. https://doi.org/10.6075/J0SJ1KT8

Rosso, I., Hogg, A. M. C., Kiss, A. E., & Gayen, B. (2015). Topographic influence on submesoscale dynamics in the Southern Ocean. *Geophysical Research Letters*, *42*(4), 1139–1147. https://doi.org/10.1002/2014GL062720

Rosso, I., Hogg, A. M. C., Strutton, P. G., Kiss, A. E., Matear, R., Klocker, A., & Van Sebille, E. (2014). Vertical transport in the ocean due to sub-mesoscale structures: Impacts in the Kerguelen region. *Ocean Modelling*, *80*, 10–23. https://doi.org/10.1016/j.ocemod.2014.05.001

Sallée, J.-B., Pellichero, V., Akhoudas, C., Pauthenet, E., Vignes, L., Schmidtko, S., et al. (2021). Summertime increases in upper-ocean stratification and mixed-layer depth. *Nature*, *591*(7851), 592–598. https://doi.org/10.1038/s41586-021-03303-x

Siegelman, L., Klein, P., Rivière, P., Thompson, A. F., Torres, H. S., Flexas, M., & Menemenlis, D. (2020). Enhanced upward heat transport at deep submesoscale ocean fronts. *Nature Geoscience*, *13*(1), 50–55. https://doi.org/10.1038/s41561-019-0489-1

Siegelman, L., Klein, P., Thompson, A. F., Torres, H. S., & Menemenlis, D. (2020). Altimetry-based diagnosis of deep-reaching sub-mesoscale ocean fronts. *Fluid*, *5*(3), 145. https://doi.org/10.3390/fluids5030145

Stommel, H. (1979). Determination of water mass properties of water pumped down from the Ekman layer to the geostrophic flow below. *Proceedings of the National Academy of Sciences*, *76*(7), 3051–3055. https://doi.org/10.1073/pnas.76.7.3051

Stukel, M. R., & Ducklow, H. W. (2017). Stirring up the biological pump: Vertical mixing and carbon export in the Southern Ocean: Vertical mixing and carbon export in SO. *Global Biogeochemical Cycles*, *31*(9), 1420–1434. https://doi.org/10.1002/2017GB005652

Tailleux, R. (2021). Spiciness theory revisited, with new views on neutral density, orthogonality, and passiveness. *Ocean Science*, *17*(1), 203–219. https://doi.org/10.5194/os-17-203-2021

The Matplotlib Development Team. (2023). Matplotlib (version v3.7.1). [software]. https://doi.org/10.5281/ZENODO.7697899. *Zenodo*.

The Pandas Development. (2023). Pandas (version v1.5.3). [software]. https://doi.org/10.5281/ZENODO.7549438. *Zenodo*.

The Seaborn Development Team. (2022). Seaborn (version v0.12.2). [software]. https://doi.org/10.5281/ZENODO.7495530. *Zenodo*.

The Xarray Development Team. (2022). Xarray (Version v2022.10.0). [software]. https://doi.org/10.5281/ZENODO.7195919. *Zenodo*.

References From the Supporting Information

Briggs, N., Perry, M. J., Cetinić, I., Lee, C., D'Asaro, E., Gray, A. M., & Rehm, E. (2011). High-resolution observations of aggregate flux during a sub-polar North Atlantic spring bloom. *Deep Sea Research Part I: Oceanographic Research Papers*, *58*(10), 1031–1039. https://doi.org/10.1016/j.dsr.2011.07.007